ISBN: 978-3-95450-214-1 ISSN: 2673-5490 doi:10.18429/JACoW-IPAC2021-TUPAB076

HIGH-GRADIENT BREAKDOWN STUDIES OF AN X-BAND ACCELERATING STRUCTURE OPERATED IN THE REVERSED TAPER DIRECTION

X. Wu*, N. Catalán-Lasheras, A. Grudiev, W. Wuensch, I. Syratchev, M. Boronat, A. V. Edwards, W. L. Millar, A. Castilla, G. McMonagle, CERN, Geneva, Switzerland

Abstract

The results of high-gradient tests of a tapered X-band traveling-wave accelerator structure powered in reversed direction are presented. Powering the tapered structure from the small aperture, normally output, at the end of the structure provides unique conditions for the study of gradient limits. This allows high fields in the first cell for a comparatively low input power and a field distribution that rapidly falls off along the length of the structure. A maximum gradient of 130 MV/m in the first cell at a pulse length of 100 ns was reached for an input power of 31.9 MW. Details of the conditioning and operation at high-gradient are presented. Various breakdown rate measurements were conducted at different power levels and rf pulse widths. The structure was standard T24 CLIC test structure and was tested in Xbox-3 at CERN.

INTRODUCTION

The CLIC collaboration is aiming at developing and testing high-gradient accelerating structures for the CLIC main linac [1, 2]. The target accelerating gradient for the 3 TeV center of mass energy version of CLIC is 100 MV/m [3]. The baseline design, named "CLIC-G", operates at 11.994 GHz in $2\pi/3$ modes at an accelerating gradient of 100 MV/m [4,5]. The high-gradient technology from CLIC has also recently been applied in future XFEL design (CompactLight), medical accelerators (FLASH), and many other facilities [6–9].

Vacuum arcing in the structures, also referred to as rf breakdown, is the major limitation to the achievable gradient in room-temperature accelerating structures. Rf breakdown will lower beam quality and damage the structure surface [10, 11]. The CLIC high-gradient specification states a maximum breakdown rate (BDR) of 3×10^{-7} breakdowns per pulse per meter at an acceleration gradient of 100 MV/m and a pulse width of 250 ns [1].

A CLIC prototype structure named "T24" was manufactured at CERN and was recently high-gradient tested in the Xbox-3 test-stand at CERN. Tests were done without the presence of a particle beam. The structure is iris-tapered, constant gradient, traveling-wave with 24 accelerating cells. Similar to the CLIC-G design, it operates at 11.994 GHz in $2\pi/3$ modes. The T24 design consists of cylinder cells which does not include the damping waveguides [1, 4, 12–14]. It reached an average gradient of 100 MV/m at the input power of 37.2 MW and the gradient of the last cell is 107 MV/m. The gradient was limited by the capability of the test-stand. However, powering the T24 from what is normally the output, provides unique conditions for the study of gradient limits. The first cell of the reversed structure reaches a given gradient with a lower power. For comparison, a gradient of 107 MV/m requires only an input power of 21.6 MW. The reversed T24 structure was named "42T" and high-gradient tested in Xbox-3 test-stand at CERN. The comparison of the field distributions of T24 and 42T is shown in Fig. 1. The test-stand and operational algorithms are presented in this paper followed by the test results and breakdown rate measurements.

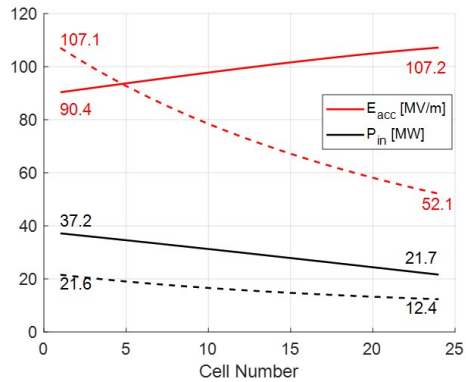

Figure 1: Field profiles of T24 (solid line) and 42T (dash line). The input power for T24 and 42T are 37.2 MW and 21.6 MW respectively. The red curve shows the accelerating gradient and the black curve the input power.

HIGH-POWER TEST-STAND AND OPERATIONAL ALGORITHMS

Diagnostic System of Xbox-3

After the move of part of the Xbox-3 to Melbourne University [15] early last year, two *X*-band klystrons and two testing slots remain at CERN. Xbox-3 combines two klystrons' rf power into two testing slots. The testing facility is shown in Fig. 2.

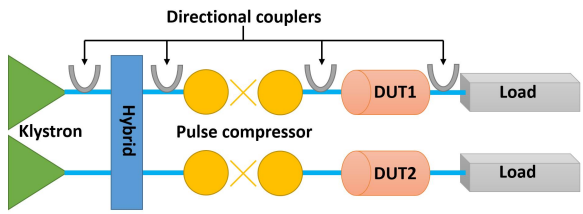

Figure 2: Schematic of the high power rf network of half of Xbox-3.

* xiaowei.wu@cern.ch

ISBN: 978-3-95450-214-1 ISSN: 2673-5490 doi:10.18429/JACoW-IPAC2021-TUPAB076

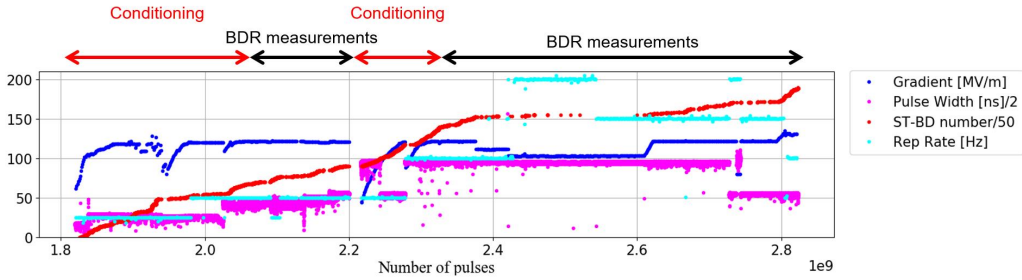

Figure 3: High-gradient testing history of 42T. The plot shows the accelerating gradient of the first cell (blue), pulse lengths (magenta), cumulative number of breakdowns (red), and repetition rate (cyan) versus the number of pulses.

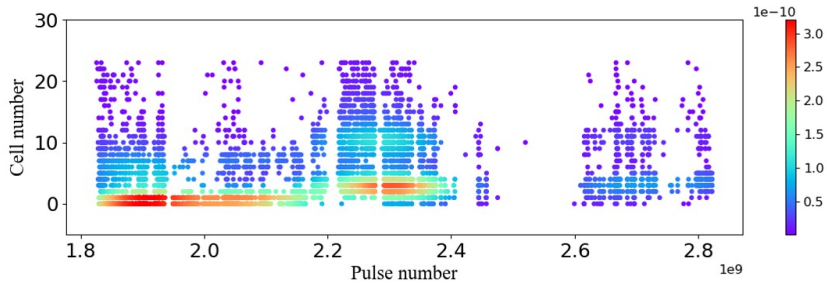

Figure 4: Breakdown positions of 42T versus the number of pulses during the high-gradient test.

The pulsed rf power is produced by combining two klystrons with a hybrid to reach a maximum of 12 MW with a repetition rate of 400 Hz [16]. We use pulse compression in Xbox-3 which allows the production of 45 MW for a 200 ns pulse [17]. Note that a phase ramp modulation is applied to the klystron pulse which generates a flat top for the compressed pulse. The phase into the klystrons is changed every pulse to direct the power to one of the two branches after the hybrid. The high repetition rate rf power is used to feed the testing slots sequentially with a final maximum repetition rate of 200 Hz.

Operational Algorithm

The control system of Xbox-3 increases the rf power to the target value automatically at a fixed pulse width. Once the target power value is reached, the pulse width is lengthened. Then, input rf power is ramped from a few hundred kilowatts again for the new pulse width.

Diagnostics used in the experiment include directional couplers to monitor the incident and reflected rf signals along the test line shown in Fig. 2 and two Faraday cups to collect upstream and downstream dark currents during rf conditioning. These signals were monitored pulse by pulse for breakdown detection. The interlock system inhibited the subsequent pulse when any jump in reflected rf signal or Faraday cup signal above a set threshold was detected. Additionally, vacuum and temperature signals were also monitored by the interlock system. As both lines share the interlock system, an interlock in one testing line stops the RF pulsing in both lines [18]. Then, the system is paused for several tens of seconds before the subsequent rf pulse, which is sufficiently long to allow the gas pressure to recover and to save the waveforms. These interlock events might indicate a breakdown event and are checked during offline data analysis. The system reduces the rf power after interlock detection and ramps the power up again.

SUMMARY OF THE HISTORY PLOT

The high-gradient testing history of 42T is shown in Fig. 3. The blue, magenta, red, and cyan dots represent accelerating gradient of the first cell, rf pulse width, cumulative number of breakdowns, and repetition rate respectively.

The gradient of the first cell reached 130 MV/m at the end of the high-gradient test. Figure 4 presents the positions of the breakdowns during the high-gradient test. The breakdowns occurred mainly in the first several cells which is consistent with the field profiles being highest in the front of the structure. The next steps are going to be a bead-pull measurement after the high-gradient test and eventually a post-mortem analysis.

BDR MEASUREMENTS

The BDR value is defined as breakdown number divided by the number of accumulated pulses. BDR measurements were conducted at different input powers and pulse widths after the structure was conditioned, as shown in Fig. 3. The input pulse shape was kept constant during the measurement and the number of breakdowns was counted. The results of the BDR measurements are summarized in Table 1.

The BDR is strongly dependent on E_{acc} and rf pulse width. The dependencies that have been observed in many CLIC prototype structures are reported in Ref. [19] and can be

ISBN: 978-3-95450-214-1 ISSN: 2673-5490 doi:10.18429/JACoW-IPAC2021-TUPAB076

Table 1: BDR Measurements of 42T

	Gradient in First Cell [MV/m]	Pulse Width [ns]	Breakdown Number	Pulse Number
BDR1	119.8	109.6	70	1.465e7
BDR2	120.8	192.3	610	4.511e7
BDR3	110.4	190.4	45	4.413e7
BDR4	102.0	188.5	11	1.519e8
BDR5	120.5	189.6	638	1.053e8
BDR6	120.8	109.1	69	4.985e7
BDR7	129.6	109.6	591	1.757e7

approximated with the following relation:

$$\frac{BDR}{{E_{\mathrm{acc}}}^{30}\tau^5} = constant, \quad (1)$$

where E_{acc} is the unloaded accelerating gradient and τ is the rf pulse width. The factor over E_{acc} of the first cell is 28.5 and 32.1 by fitting the results of the 190 ns and 110 ns BDR measurements respectively, as shown in Fig. 5.

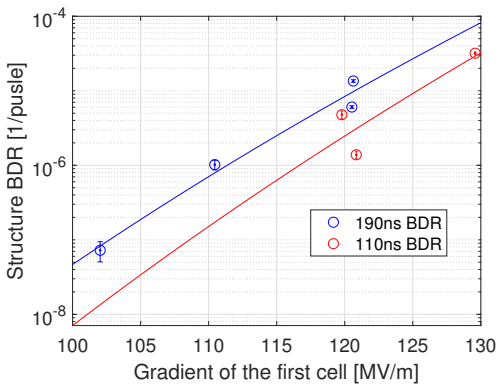

Figure 5: Breakdown rate measurements results with the fit curve. Blue and red dots present the BDR measurements of 190 ns and 110 ns rf pulse width.

The BDR dependency on rf pulse width can be calculated from the BDR5 and BDR6 result from Table 1. It indicated the factor over rf pulse width is 2.67 by fitting the two results.

CONCLUSION

The results of high-gradient tests of a tapered X-band traveling-wave accelerator structures powered in reversed direction named 42T are presented. The first cell of 42T reached a maximum low-breakdown-rate gradient of 130 MV/m at a pulse length of 100 ns in the test with a relatively lower input power of 31.9 MW. Various breakdown rate measurements were conducted at different power level and rf pulse width. The BDR dependencies on accelerating gradient and rf pulse width were studied. The factors over the first cell gradient are 28.5 and 32.1 by fitting the results of the 190 ns and 110 ns BDR measurements. Bead-pull measurement and post-mortem analysis will be conducted in the future.

REFERENCES

[1] M. Aicheler *et al.*, "A Multi-TeV Linear Collider Based on CLIC Technology: CLIC Conceptual Design Report", CERN, Geneva, Switzerland, Rep. CERN-2012-007, 2012.

[2] M. Boland *et al.*, "Updated baseline for a staged Compact Linear Collider", CERN, Geneva, Switzerland, Rep. CERN-2016-004, Aug. 2016.

[3] R. Tomás, "Overview of the compact linear collider", *Phys. Rev. ST Accel. Beams*, vol. 13, p. 014801, Jan. 2010. doi:10.1103/PhysRevSTAB.13.014801

[4] A. Grudiev and W. Wuensch, "Design of the CLIC Main Linac Accelerating Structure for CLIC Conceptual Design Report", in *Proc. 25th Linear Accelerator Conf. (LINAC'10)*, Tsukuba, Japan, Sep. 2010, paper MOP068, pp. 211-213.

[5] H. Zha and A. Grudiev, "Design and optimization of compact linear collider main linac accelerating structure", *Phys. Rev. Accel. Beams*, vol. 19, p. 111003, Nov. 2016. doi:10.1103/PhysRevAccelBeams.19.111003

[6] A. A. Aksoy *et al.*, "Conceptual Design of a X-FEL Facility using CLIC X-band Accelerating Structure", in *Proc. 5th Int. Particle Accelerator Conf. (IPAC'14)*, Dresden, Germany, Jun. 2014, pp. 2914-2917. doi:10.18429/JACoW-IPAC2014-THPRO025

[7] G. D'Auria, "Compact light proposal", presented at the 10th Int. Workshop on Breakdown Science and High Gradient Technology (HG2017), Valencia, Spain, Jun. 2017, unpublished.

[8] W. Fang *et al.*, "R&D of X-band Accelerating Structure for Compact XFEL at SINAP", in *Proc. 27th Linear Accelerator Conf. (LINAC'14)*, Geneva, Switzerland, Aug.-Sep. 2014, paper TUPP127, pp. 715-718.

[9] M. Diomede *et al.*, "Preliminary rf design of an X-band linac for the EuPRAXIA@SPARC_LAB project", *Nucl. Instrum. Methods Phys. Res., Sect. A*, vol. 909, pp. 243–246, Nov. 2018. doi:10.1016/j.nima.2018.01.032

[10] J. Wang and G. Loew, "Field emission and RF breakdown in high-gradient room-temperature linac structures", SLAC, Menlo Park, CA, USA, Rep. 7684, 1997.

[11] A. Palaia, M. Jacewicz, R. Ruber, V. Ziemann, and W. Farabolini, "Effects of rf breakdown on the beam in the compact linear collider prototype accelerator structure", *Phys. Rev. ST Accel. Beams*, vol. 16, p. 081004, Aug. 2013. doi:10.1103/PhysRevSTAB.16.081004

ISBN: 978-3-95450-214-1 ISSN: 2673-5490 doi:10.18429/JACoW-IPAC2021-TUPAB076

[12] X. Wu *et al.*, "High-gradient breakdown studies of an Xband compact linear collider prototype structure", *Phys. Rev. Accel. Beams*, vol. 20, p. 052001, May 2017. doi:10.1103/PhysRevAccelBeams.20.052001

[13] W. Wuensch *et al.*, "Experience Operating an X-band High-Power Test Stand at CERN", in *Proc. 5th Int. Particle Accelerator Conf. (IPAC'14)*, Dresden, Germany, Jun. 2014, pp. 2288-2290. doi:10.18429/JACoW-IPAC2014-WEPME016

[14] T. Higo *et al.*, "Comparison of High Gradient Performance in Varying Cavity Geometries", in *Proc. 4th Int. Particle Accelerator Conf. (IPAC'13)*, Shanghai, China, May 2013, paper WEPFI018, pp. 2741-2743.

[15] M. Volpi *et al.*, "The Southern Hemisphere's First X-Band Radio-Frequency Test Facility at the University of Melbourne", presented at the 12th Int. Particle Accelerator Conf. (IPAC'21), Campinas, Brazil, May 2021, paper WEPAB374, this conference.

[16] N. Catalan-Lasheras *et al.*, "Commissioning of XBox-3: A Very High Capacity X-band Test Stand", in *Proc. 28th Linear Accelerator Conf. (LINAC'16)*, East Lansing, MI, USA, Sep. 2016, pp. 568-571. doi:10.18429/JACoW-LINAC2016-TUPLR047

[17] N. Catalan-Lasheras *et al.*, "High Power Conditioning of X-Band RF Components", in *Proc. 9th Int. Particle Accelerator Conf. (IPAC'18)*, Vancouver, Canada, Apr.-May 2018, pp. 2545-2548. doi:10.18429/JACoW-IPAC2018-WEPMF074

[18] M. Volpi *et al.*, "High Power and High Repetition Rate X-band Power Source Using Multiple Klystrons", in *Proc. 9th Int. Particle Accelerator Conf. (IPAC'18)*, Vancouver, Canada, Apr.-May 2018, pp. 4552-4555. doi:10.18429/JACoW-IPAC2018-THPMK104

[19] A. Grudiev, S. Calatroni, and W. Wuensch, "New local field quantity describing the high gradient limit of accelerating structures", *Phys. Rev. ST Accel. Beams*, vol. 12, p. 102001, Oct. 2009. doi:10.1103/PhysRevSTAB.12.102001